Joule

CellPress

Article

Identifying the Soft Nature of Defective Perovskite Surface Layer and Its Removal Using a Facile Mechanical Approach

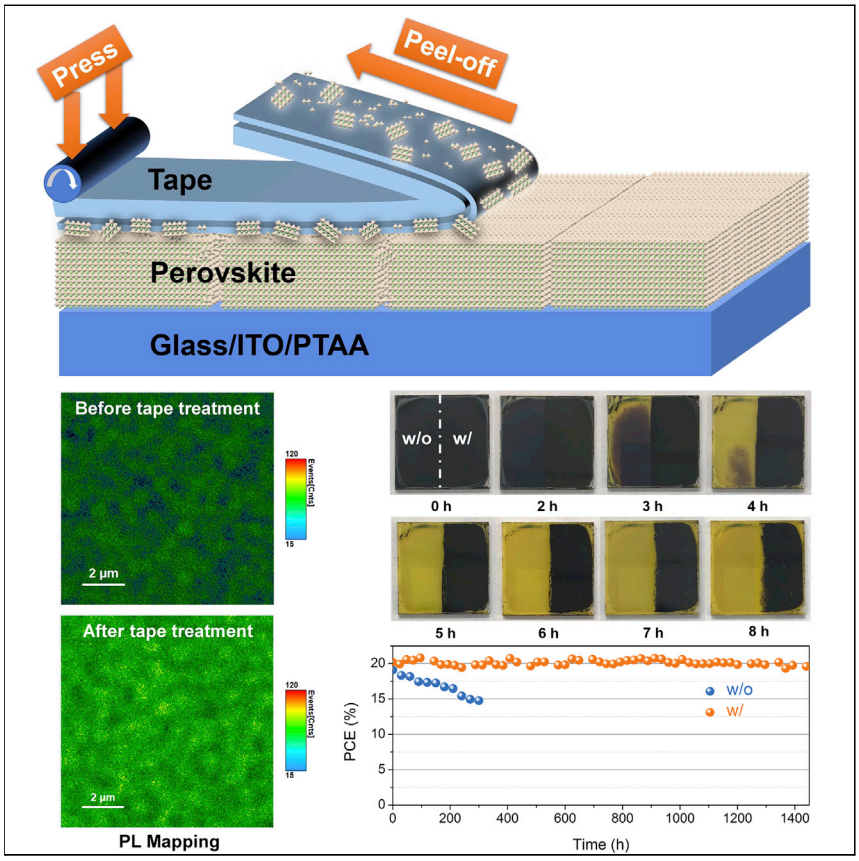

Chen and co-workers report a facile method for the removal of defective perovskite surface layers with adhesive tapes. This strategy is based on the discovery that the defective surface layer is mechanically softer and has weaker bonding to the crystalline layer underneath it. The adhesive tape has appropriate bonding with perovskites and, thus, removes the defective surface layer without damaging the crystalline regions. The tape treatment can stabilize commonly used perovskite compositions and is compatible with the scaling up of perovskite solar modules.

Shangshang Chen, Ye Liu, Xun Xiao, ..., Xuezeng Dai, Zhenyi Ni, Jinsong Huang

jhuang@unc.edu

HIGHLIGHTS

Perovskite defective surface layers are mechanically softer than crystalline regions

Adhesive tape can remove defective surface layers and stabilize perovskite devices

Tape treatment is compatible with the scaling up of perovskite solar modules

Chen et al., Joule 4, 1–14
December 16, 2020
https://doi.org/10.1016/j.joule.2020.10.014

Please cite this article in press as: Chen et al., Identifying the Soft Nature of Defective Perovskite Surface Layer and Its Removal Using a Facile Mechanical Approach, Joule (2020), https://doi.org/10.1016/j.joule.2020.10.014

Joule

CellPress

Article

Identifying the Soft Nature of Defective Perovskite Surface Layer and Its Removal Using a Facile Mechanical Approach

Shangshang Chen,[1] Ye Liu,[1] Xun Xiao,[1] Zhenhua Yu,[1] Yehao Deng,[1] Xuezeng Dai,[1] Zhenyi Ni,[1] and Jinsong Huang[1,2,*]

SUMMARY

The presence of a defective layer composed of nanocrystals and amorphous regions at the surface of perovskite films has been shown to initialize the degradation of perovskites and cause nonradiative recombination. Here, we report the discovery that these defective surface layers are mechanically softer than the crystalline regions. The defective surface layer has a weaker bonding with the crystalline layer underneath it, which enables a facile approach to mechanically peel-off these defective layers using adhesive tapes. The chosen low-cost tape has an appropriate bonding force with perovskites, so the peeling does not damage the crystalline region and embedded interfaces underneath. The tape-treated devices retained 97.1% of the initial efficiency after operation at the near maximum power point under one sun illumination for 1,440 h at 65°C. This method is universally effective in enhancing the stability of various commonly used perovskite compositions and is compatible with the scaling up of perovskite solar modules.

INTRODUCTION

Metal halide perovskites (MHPs) have demonstrated remarkable progress in photovoltaic power conversion efficiency (PCE) from 3.8% to 25.2% in less than one decade,[1] showing their great potential as the next-generation low-cost solar technology. Among all the remaining issues to be addressed, poor stability is the most outstanding challenge that needs both fundamental understanding and engineering improvement toward the commercialization of perovskite photovoltaics.[2] In the past few years, the stability of perovskite solar cells (PSCs) has been dramatically improved with global efforts dedicated to tuning perovskite compositions,[3] passivating perovskite defects,[4] constructing stable heterostructures,[5] and developing better encapsulation methods compatible with perovskite materials.[6] Meanwhile, the perovskite community is gaining a deeper understanding of the structural features that cause the degradation of perovskites, which, in turn, can significantly guide the stabilization of PSCs. Recently, we reported the discovery of a defective layer composed of disconnected nanocrystals and amorphous phases at the surface of apparent single crystalline grains in polycrystalline perovskite films by solution deposition methods and such a defective layer was observed to initialize and accelerate the degradation of PSCs (unpublished data). The accelerated degradation is not caused by excess PbI_2 because red light, which PbI_2 does not absorb, also accelerates the degradation when the defective layer is present. Therefore, eliminating such a defective surface layer is an essential step for stabilizing PSCs and modules. Currently, removing the defective perovskite surfaces by vacuum-assisted

Context & Scale

The defective perovskite surface layer composed of nanocrystals and amorphous regions has been shown to initialize the degradation of perovskites. To stabilize perovskite materials and devices, it is essential to remove such a defective surface layer. Herein, we studied the mechanical properties of the perovskite surface layer and found that such a defective layer is softer than the crystalline regions and has weaker bonding to the crystalline layer underneath. Based on this discovery, we report a simple strategy to remove the soft, defective surface layer with low-cost adhesive tapes. The adhesive tape has appropriate bonding with perovskites and, thus, removes the defective surface layer without damaging the underlying crystalline regions. This method has also shown the universality in commonly used perovskite compositions and the compatibility with scaling up of perovskite photovoltaics.

Please cite this article in press as: Chen et al., Identifying the Soft Nature of Defective Perovskite Surface Layer and Its Removal Using a Facile Mechanical Approach, Joule (2020), https://doi.org/10.1016/j.joule.2020.10.014

solid-phase recrystallization or polishing processes has been demonstrated to enhance the stability and efficiency of PSCs.[7,8] However, these strategies are appropriate for small-area PSCs but are not compatible with the scalable, high-speed manufacturing of large-area perovskite photovoltaic modules, particularly those made by roll-to-roll processes and have strict requirements for substrate flatness and perovskite material thickness. Therefore, it is important to develop an effective stabilization method that is compatible with the high-throughput manufacturing of perovskite modules without significantly increasing production cost, as low-cost and high-throughput processability is one major advantage of perovskite photovoltaics in competing with conventional counterparts.[9–14]

In this work, we report a facile method for removing defective surface layers using low-cost adhesive tapes that is compatible with scalable manufacturing of perovskite photovoltaic modules. This method is based on our observation that MHP polycrystalline films with various compositions show an interruption of lattice continuity on the film surfaces. The top surfaces have a typical morphology of many nanocrystals surrounded by an amorphous phase. Such defective surfaces with higher density dangling chemical bonds and vacancies than crystalline regions in the grain interior are found to have weaker bonding with underlying crystalline grains. The weaker mechanical strength at the defective surface regions compared with that at the crystalline regions and the relatively soft nature of perovskites allow the mechanical peeling off of these defective surface layers by low-cost adhesive tapes—demostrated herein for the first time. This simple, high-throughput, and low-cost tape treatment significantly enhanced the stability of perovskites. In addition, the adhesive residual is shown to passivate the perovskites, boosting the efficiency of p-i-n structure solar cells to 22.0%.

RESULTS AND DISCUSSION

The mechanical properties of the defective perovskite surface have barely been studied in the past. To characterize the mechanical properties of the defective surface layer on the top of grains, we performed a nanoscratch test on both pristine and polished $MAPbI_3$ films.[15–17] The $MAPbI_3$ films with a thickness of ~600 nm were fabricated by spin-coating and were verified to yield a device efficiency over 19.0% using a p-i-n device structure before the nanoscratch test.[18] In the nanoscratch test, a tip was used to scratch the perovskite films from the top surface to the film interior with a penetration depth of 30 nm while moved laterally for ~500 nm, as illustrated in Figure 1A. The lateral force of the tip was recorded, which should reflect the bonding strength at different probing depths. The measurement has been conducted on four groups of pristine and surface-polished films, and the results were statistically analyzed. As shown in Figure 1B, the lateral force measured in the pristine $MAPbI_3$ film increases almost linearly with the scratching depth, which was controlled by gradually increasing the normal load. After the nanocrystal/amorphous phase top layer was polished off, the lateral force was larger than that in the pristine film at all scratch depths, indicating that the defective surface layers have less adhesion to the region underneath than the crystalline grain interiors. The averaged lateral force on four different polished films was ~50% larger than that on the pristine films, and this result verifies the weaker adhesion of the defective surface layers to the underlining crystalline regions compared with inside the crystalline region.

Based on this observation, we designed a method to remove the defective layer with adhesive tapes, while the underlying crystalline region remains unaffected, by utilizing the weaker adhesion of the defective region to crystalline regions and the relatively soft nature of MHPs, which is due to the weak ionic bonding between

[1]Department of Applied Physical Sciences, University of North Carolina at Chapel Hill, Chapel Hill, NC 27599, USA

[2]Lead Contact

*Correspondence: jhuang@unc.edu

https://doi.org/10.1016/j.joule.2020.10.014

Please cite this article in press as: Chen et al., Identifying the Soft Nature of Defective Perovskite Surface Layer and Its Removal Using a Facile Mechanical Approach, Joule (2020), https://doi.org/10.1016/j.joule.2020.10.014

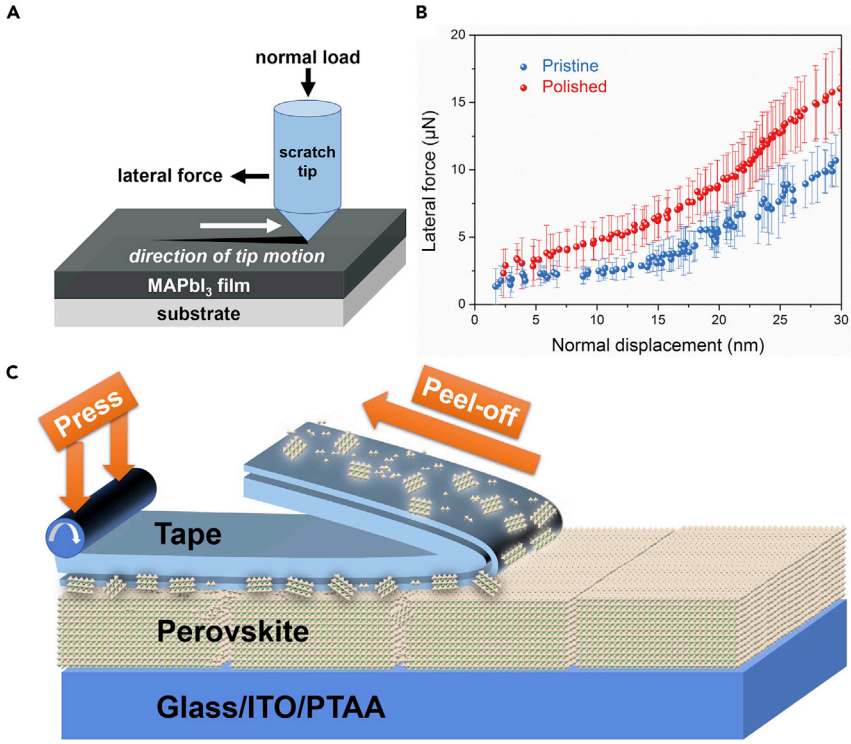

Figure 1. Removing Defective Surface Layers with Adhesive Tape

(A) The setup of nanoscratch test.

(B) Nanoscratch results of the pristine and polished $MAPbI_3$ films. Data are represented as mean ± SEM for four samples.

(C) Schematic of peeling an adhesive tape off a $MAPbI_3$ film.

the large-size metal cations and halide anions.[5,19,20] As illustrated in Figure 1C, an adhesive tape made of soft adhesive on a flexible polymer substrate is pressed onto the rough and defective perovskite surfaces to form an intimate contact with appropriate bonding strength. After peeling off this adhesive material, nanocrystals and the amorphous phase were retained on the tape and were, thus, removed from perovskite films. One prerequisite for the success of this method is that the bonding of perovskite large grains with the charge-transport-layer-covered indium tin oxide (ITO) substrate should be strong enough so that the large grains are not peeled off. To demonstrate this, tape treatment was performed by pressing a low-cost 3M Temflex 1700[21] adhesive tape onto pristine $MAPbI_3$ films and subsequently separating the tape from the $MAPbI_3$ surfaces at an angle of ~180° to the film surface, as schematically illustrated in Figure 1C. Video S1 shows this peeling process. The cross-sectional scanning electron microscopy (SEM) image in Figure S1 shows that the tape forms gapless intimate contact with perovskite films after pressing the tape at a small pressure of 1 MPa at room temperature. Using the 180° peel method[22], the adhesive strength between the tape and pristine perovskite surfaces was measured to be 2.3 ± 0.1 N cm^{-1}. The peeling-off force was increased to 2.6 ± 0.1 N cm^{-1} when the tape was applied a second or third time, indicating the successful peeling of the defective region during the first peeling-off process.

To verify that the tape treatment can effectively remove the nanocrystals and amorphous phase on the perovskite film surfaces, we conducted high-resolution transmission electron microscopy (HRTEM) measurement of tape-treated $MAPbI_3$ solar cells

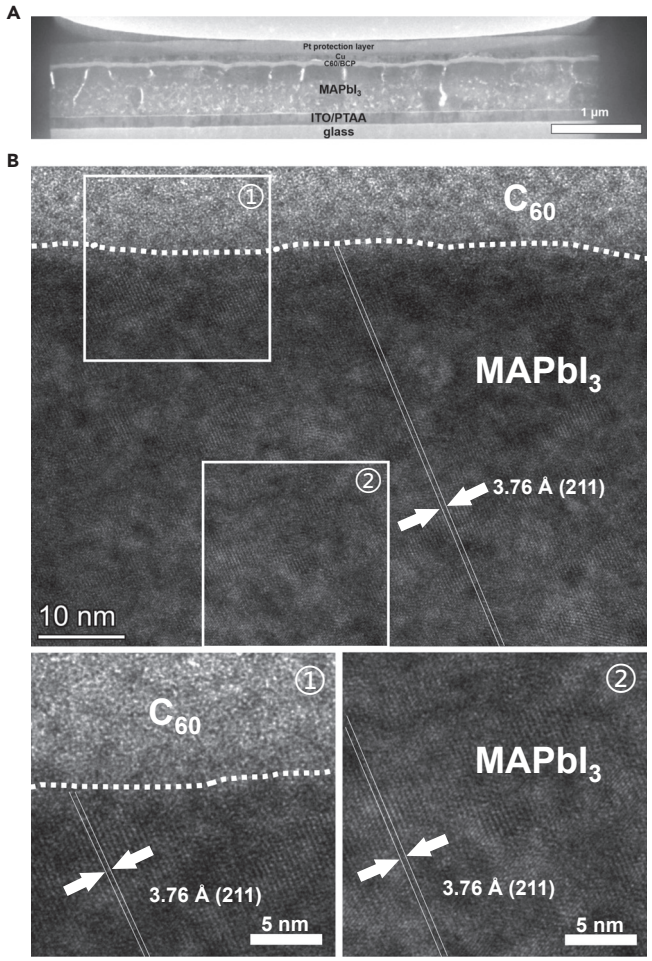

Figure 2. Transmission Electron Microscopy Characterization

(A) Cross-section FIB lamellae for TEM analysis.

(B) Cross-section HRTEM images of the perovskite/C_{60} interface of tape-treated $MAPbI_3$ device. The squares highlight the perovskite-C_{60} interface (position 1) and the grain interior (position 2) regions.

that contain both an electron transport layer and a metal electrode. One representative image is shown in Figure 2B and twelve others at randomly selected locations in a 6 μm-long focused ion beam (FIB) lamellae of the same device are shown in Figure S2, respectively. No nanocrystal or amorphous phase was observed at the perovskite top surface in any of these HRTEM images. The perovskite lattices inside the grains were found to be continuous and extended directly to the perovskite/C_{60} interface without the presence of obvious extended defects. To illustrate this, we zoomed-in on region 2, which is 50 nm away from perovskite/C_{60} interface and region 1, which is at the perovskite-C_{60} interface, and we marked the (211) plane in the figure. The same trend was also observed at twelve other locations, shown in Figure S2. This result confirms the effectiveness of adhesive tape in removing the defective surface layers. In addition, we carried out energy dispersive spectroscopy (EDS) measurement to analyze the perovskite residuals on the tape after peeling. Both lead and iodide were detected on the tape with an atomic ratio of ~1:3 (Figure S3 and Table S1). The surface topography changes of the $MAPbI_3$ films caused by tape treatment were characterized via both atomic force microscopy (AFM) and top-view SEM. As shown in Figure S4, AFM measurement results show that the

overall topography of the $MAPbI_3$ film did not change notably, while the film became slightly smoother after tape treatment with the root mean square (RMS) roughness reduced from 11.39 to 9.15 nm after peeling. This also indicates an advantage of tape treatment over polishing; the soft adhesive can have conformal contact with the non-flat film surfaces, which allows for the removal of the defective layers without the need to flatten the whole films. This is particularly attractive for applications where the retention of the surface textures is preferred, such as perovskite/silicon tandem solar cells. No pinhole in the film was observed in the SEM image of tape-treated $MAPbI_3$ surfaces (Figure S5), indicating the bonding between large grains and poly(bis(4-phenyl)(2,4,6-trimethylphenyl)amine) (PTAA)-coated ITO is stronger than that between the defective layer and the crystalline region.

We further investigated the effectiveness and uniformity of tape treatment by carrying out multiple structural, optoelectrical, and mechanical characterizations. First, the crystallinity of surface perovskites was examined via grazing incidence X-ray diffraction (GIXRD) on the same $MAPbI_3$ film before and after tape treatment. As shown in Figure 3A, the diffraction peak intensity of all crystallographic planes increased significantly after tape treatment, confirming the exposure of the crystalline region by successful removal of nanocrystals or amorphous surfaces. Subsequently, the activation energy (E_a) for ion migration of the $MAPbI_3$ films was measured via temperature-dependent dark conductivity. Lateral structure devices were fabricated by evaporating two Au electrodes on glass/PTAA/$MAPbI_3$ films, which is shown in the inset of Figure 3B. The E_a can be extracted from the Nernst-Einstein equation: $\sigma(T) = (\sigma_0/T)\exp(-E_a/k_B T)$, where k_B is Boltzmann constant, σ_0 is a constant, and T is temperature. The applied electric field was 0.4 V μm^{-1}, which is close to that in the operational solar cells. As shown in Figure 3B, the conductivity can be well separated into electronic conduction and ionic conduction regions for both cases, which is typical for $MAPbI_3$.[23,24] For the film without tape surface treatment, the ionic conductivity, with an E_a of 0.31 $\pm$ 0.02 eV, started to dominate the total conductivity when the temperature increased to 241 K. In striking contrast, the tape-treated film exhibited an increased transition temperature of 273 K and a larger E_a of 0.71 $\pm$ 0.03 eV, indicating that ion migration was greatly suppressed through the elimination of defective surfaces that acted as the high-speed ion-migration channel. The surface mechanical properties of pristine and tape-treated $MAPbI_3$ films were studied with a nanoindenter. The indentation depth of a Berkovich tip used in this measurement was fixed within 10% of the total film thickness to avoid the impact from the substrate.[25] As shown in Figure 3C, the surface of the pristine $MAPbI_3$ exhibited a hardness of 0.54 $\pm$ 0.03 GPa, and the surface hardness increased to 0.64 $\pm$ 0.05 GPa after tape treatment. This again proves that pristine perovskite surfaces with defective surface layers are softer than the underlying high-crystallinity grain interior, and the softer surface should result from the dangling chemical bonds and high-density defects on the film surface.[15,16] We then mapped steady-state photoluminescence (PL) of the same $MAPbI_3$ film before and after tape treatment to examine the uniformity of tape treatment. As shown in Figure 3D, the tape-treated $MAPbI_3$ film exhibited higher PL intensity in comparison to the pristine film, indicating less nonradiative recombination after eliminating the defective surfaces. In addition, almost the entire measured area exhibited enhanced PL intensity and no dark areas were observed after tape treatment, suggesting good uniformity of tape treatment in removing the defective surfaces without introducing any physical damage to the films, such as peeling off any grains from the film surface.

PSCs were fabricated with a p-i-n planar heterojunction configuration of ITO/PTAA/perovskites/C_{60}/bathocuproine (BCP)/Cu. $MAPbI_3$ films were deposited onto the

Please cite this article in press as: Chen et al., Identifying the Soft Nature of Defective Perovskite Surface Layer and Its Removal Using a Facile Mechanical Approach, Joule (2020), https://doi.org/10.1016/j.joule.2020.10.014

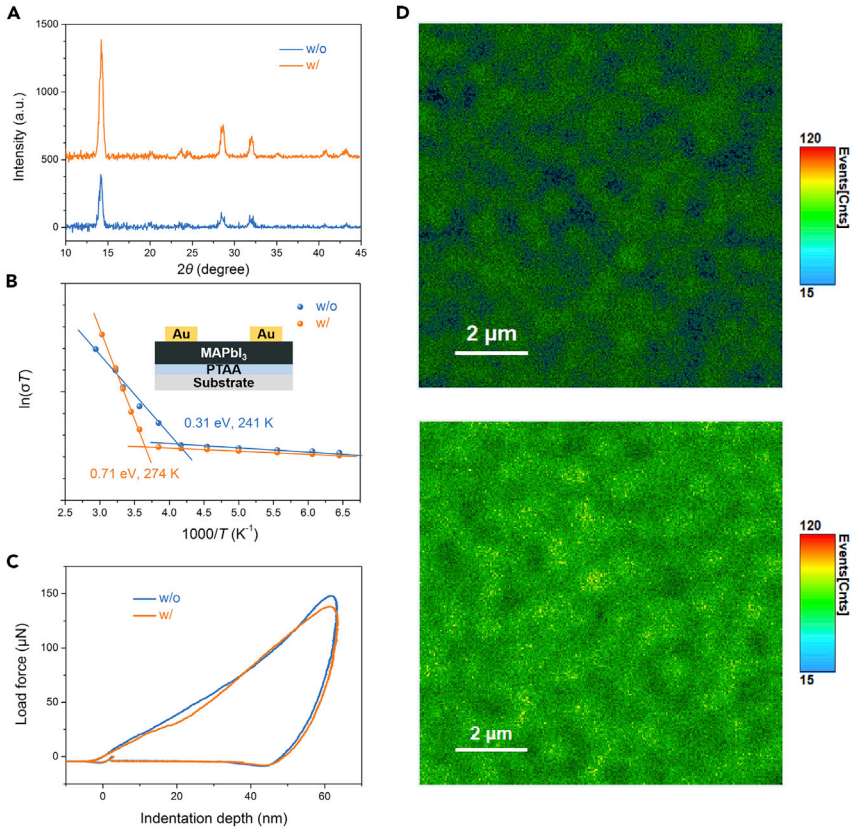

Figure 3. Structural, Optoelectrical, and Mechanical Characterizations of Perovskite Films by Tape Treatment

(A) GIXRD patterns (vertically offset for clarity) of a $MAPbI_3$ film without and with tape treatment at an incident angle of 0.1°.

(B) Temperature-dependent conductivity of the lateral structure device without and with tape treatment measured in the dark. The structure of the device for this measurement is shown in the inset.

(C) Loading and unloading force curves for $MAPbI_3$ films w/o and w/ tape treatment.

(D) PL mapping images of a $MAPbI_3$ film before (top) and after (bottom) tape treatment.

PTAA-covered ITO substrate with a one-step spin-coating process.[18] As shown in Figure 4A, the control device without tape treatment exhibited an open-circuit voltage (V_{oc}) of 1.09 V, a short-circuit current density (J_{sc}) of 22.5 mA cm^{-2}, a fill factor (*FF*) of 78.9%, and thus a PCE of 19.3%, which are consistent with previous results.[18] After tape treatment, the device delivered an enhanced V_{oc} of 1.13 V and a larger *FF* of 81.0% and a comparable J_{sc} of 22.4 mA cm^{-2}, yielding a higher PCE of 20.5% from *J-V* curve and a stabilized efficiency of 20.3% (Figure 4B). The mean PCEs are 18.8% $\pm$ 0.3% and 20.1% $\pm$ 0.3% for perovskite devices without and with tape treatment, respectively. The photovoltaic parameters of the devices with and without tape treatment were analyzed and the statistical distribution is shown in Figure S6. No noticeable hysteresis was observed under forward and reverse photocurrent sweeps (Figure S7A and Table S2), and the J_{sc} calculated from the external quantum efficiency (EQE) spectrum agreed well with that derived from the *J-V* curves (Figure S7B). The enhanced V_{oc} can be attributed to suppressed nonradiative recombination, which is supported by the enhanced PL intensity shown in Figure 3D and tripled charge recombination lifetime measured by transient photovoltage (TPV) at a light bias of 1 sun intensity (Figure 4C). A reduced trap density in

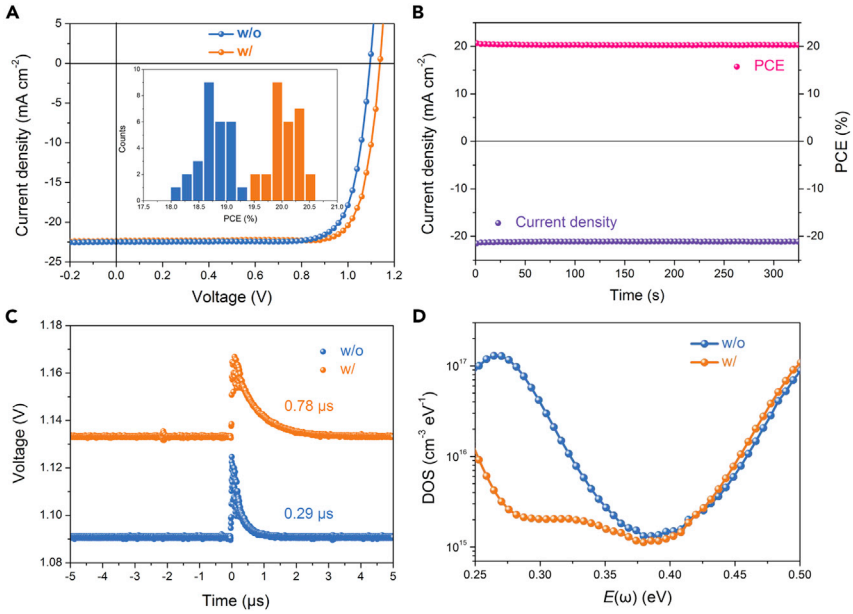

Figure 4. Performance and Characteristics of Perovskite Devices Following Tape Treatment

(A) *J-V* characteristics of the $MAPbI_3$ PSCs without and with tape treatment. Inset shows the statistics of PCE distribution for perovskite devices without and with tape treatment.

(B) Current density and steady-state power output of a best-performing $MAPbI_3$ device with tape treatment measured at a fixed bias of 0.96 V.

(C and D) TPV (C) and tDOS (D) spectra of the perovskite devices based on control and tape-treated $MAPbI_3$ films.

the tape-treated perovskite device was also discovered by the thermal admittance spectroscopy measurement result, shown in Figure 4D. The tape-treated device exhibited a much lower trap density of states (tDOS) in shallow trap depth region (0.25 to 0.35 eV). On the one hand, the reduced trap density can be attributed to the removal of defective surfaces, and one the other hand, we found that further pressing the tape onto the perovskite surface might leave a thin layer of polymer (rubber) adhesive on the top of the films, which was also observed to have passivation effects on devices. The adhesive residuals on the perovskite surfaces were confirmed by the X-ray photoelectron spectroscopy (XPS) measurement. As shown in Figure S8A, the intensity of the O_{1s} peak on the surface of a $MAPbI_3$ film increased significantly after tape treatment, which should originate from the polymer resin residues—a key component in the adhesive of tapes.[21] The XPS spectra of the tape before and after surface treatment of a $MAPbI_3$ film show both Pb and I signals (Figures S8B and S8C), which further confirms that the defective perovskite surface layer was removed by the adhesive tape. It is also very encouraging that the adhesive residual had no detrimental effect on the device efficiencies, which is consistent with our previous work that an insulating layer of many compositions also has passivation effects on perovskites due to the various type of passivation functional groups.[26,27] To quantify the passivation effect of the adhesive, we further tested the performance of the tape-treated devices with and without toluene washing. It was found the V_{oc} decreased slightly after washing off the adhesive layer with toluene (Figure S9 and Table S3). Therefore, the reduced trap density is attributable to both the removal of defective surfaces and the passivation effect of adhesive residuals. Overall, the longer carrier recombination lifetime and lower trap density of the tape-treated devices demonstrate that the tape treatment was able to effectively reduce the perovskite surface defects, accounting for the suppressed charge recombination and, thus, enhanced

Please cite this article in press as: Chen et al., Identifying the Soft Nature of Defective Perovskite Surface Layer and Its Removal Using a Facile Mechanical Approach, Joule (2020), https://doi.org/10.1016/j.joule.2020.10.014

Table 1. Photovoltaic Parameters of the PSCs with and without Tape Treatment

Composition	Tape Treatment	V_{oc} (V)	J_{sc} (mA cm^{-2})	*FF*	PCE (%)
$MAPbI_3$ (one step)	w/o	1.09	22.5	0.789	19.3
	w/	1.13	22.4	0.811	20.5
$MAPbI_3$ (two step)	w/o	1.07	21.7	0.762	17.8
	w/	1.09	21.9	0.784	18.7
$MAPbI_3$ (doctor bladed)	w/o	1.10	21.7	0.790	18.8
	w/	1.13	21.5	0.806	19.6
$Cs_{0.05}FA_{0.81}MA_{0.14}PbI_{2.55}Br_{0.45}$ (one step)	w/o	1.09	22.3	0.788	19.2
	w/	1.13	22.5	0.808	20.5
$Rb_{0.05}Cs_{0.05}FA_{0.85}MA_{0.05}PbI_{2.85}Br_{0.15}$ (one step)	w/o	1.12	23.3	0.788	20.6
	w/	1.15	23.4	0.817	22.0
$Cs_{0.40}FA_{0.60}PbI_{1.94}Br_{1.06}$ (one step)	w/o	1.19	17.5	0.820	17.1
	w/	1.24	18.6	0.763	17.6
$Cs_{0.20}FA_{0.80}Pb_{0.50}Sn_{0.50}I_3$ (one step)	w/o	0.81	31.0	0.743	18.6
	w/	0.84	31.0	0.776	20.2

device efficiency. In addition to nanocrystals and amorphous particles, we found that the adhesive tape was also very effective in removing excessive PbI_2 particles which have been reported to cause the degradation of perovskites due to photolysis effects.[28,29] As shown in Figure S10, the $MAPbI_3$ film processed from a PbI_2-excess precursor solution (PbI_2:MAI molar ratio of 1.05:1) shows white PbI_2 particles on the top surface, which were then effectively removed after treatment with the adhesive tape. Our study further provides a simple strategy to remove the excessive PbI_2, thus enhancing the light stability of perovskite films.

To further test the broad applicability of this surface treatment method, we applied this method to a set of mixed cation and halide perovskite compositions containing cesium (Cs), rubidium (Rb), or tin (Sn), as well as $MAPbI_3$ films prepared via different methods, including one-step and two-step spin-coating methods and blade-coating. The GIXRD spectra in Figure S11 show enhanced XRD peak intensity after tape treatment on all these perovskite films, indicating that there are defective layers residing on the surface of all these perovskites. This appears to be a common phenomenon for perovskite films, which is independent of compositions or preparation methods; however, the increases in peak intensity after tape treatment varied with perovskite compositions. $MAPbI_3$ films exhibited the largest XRD intensity increase after tape treatment, indicating that defective regions on the film surface form most easily on $MAPbI_3$ film. This is in accordance with the HRTEM results on a widely adopted stable composition of $Cs_{0.05}FA_{0.81}MA_{0.14}PbI_{2.55}Br_{0.45}$. Figure S12 shows the co-existence of an amorphous phase and high-crystallinity regions on the surface of $Cs_{0.05}FA_{0.81}MA_{0.14}PbI_{2.55}Br_{0.45}$ (CsFAMA) grains, while most of the $MAPbI_3$ film surfaces are covered by amorphous phase. This might be because MA cations are more volatile and escape more easily from $MAPbI_3$ surfaces during the thermal annealing process.[30,31] Subsequently, we fabricated the PSCs based on these films and detailed device performance parameters are summarized in Table 1, and the corresponding *J-V* curves are depicted in Figure S13. Obviously, the tape treatment works well on all perovskite compositions for improving efficiencies, and the highest PCE of 22.0% (stabilized PCE of 21.8%, Figure S14) was realized for $Rb_{0.05}Cs_{0.05}FA_{0.85}MA_{0.05}PbI_{2.85}Br_{0.15}$ (RbCsFAMA)-based p-i-n structure devices. It

Please cite this article in press as: Chen et al., Identifying the Soft Nature of Defective Perovskite Surface Layer and Its Removal Using a Facile Mechanical Approach, Joule (2020), https://doi.org/10.1016/j.joule.2020.10.014

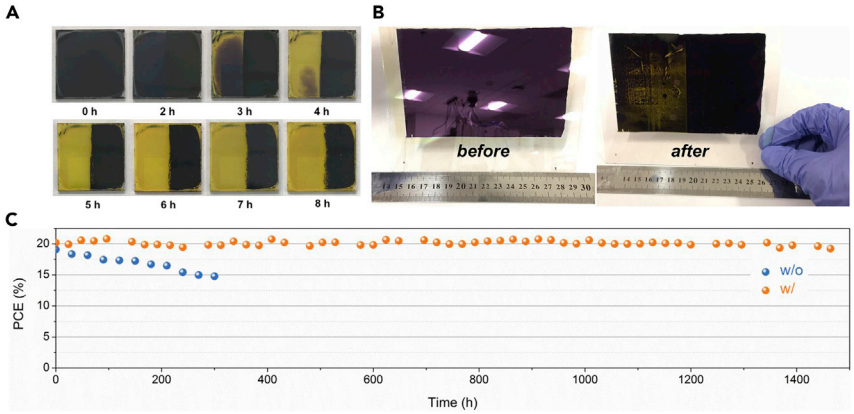

Figure 5. Stability Studies of Perovskite Films and Devices

(A) Photograph of a $MAPbI_3$ film, with an area of 15 × 15 mm prepared by a one-step spin-coating method, after light soaking for different time intervals. The right half of the film was treated with adhesive tape.

(B) Photographs of a blade-coated $MAPbI_3$ film with an area of ~100 cm^2 (surface tape treatment on the right half with a tape-wrapped roller) before and after light soaking for 3.5 h.

(C) Operational stability of encapsulated solar cells based on $Rb_{0.05}Cs_{0.05}FA_{0.85}MA_{0.05}PbI_{2.85}Br_{0.15}$ perovskite active layers without and with tape treatment.

is also noted that the tape treatment increased PCEs of Sn-containing narrow-band-gap (1.21 eV) PSCs with a composition of $Cs_{0.20}FA_{0.80}Pb_{0.50}Sn_{0.50}I_3$ from 18.6% to 20.2%, which is one of the highest PCEs reported for Pb-Sn binary PSCs to date.[32–34]

The stability of $MAPbI_3$ films prepared by a one-step method was tested under light-soaking conditions with simulated AM 1.5G irradiation. Here, only half the area of each film was treated with tape so that we could exclude the impact of film-to-film quality variation on the stability study. As presented in Figure 5A, the tape-treated right half still remained black after 8 h of light soaking, while the control half already decomposed into yellow phases in less than 4 h, showing that tape treatment can improve film light stability. On the one hand, the improved film stability can be attributed to the removal of defective surface layers. On the other hand, the aforementioned adhesive residuals that remain on the top of the films can further encapsulate the perovskite films. This is supported by the worst light stability of the film after using toluene to wash off the adhesive residue, as shown in Figure S15.

This simple surface treatment method can be used to stabilize large-area perovskite modules. To demonstrate it, we pressed tape from a wide tape roller onto a large-area (~100 cm^2) blade-coated $MAPbI_3$ film (Figure S16) and then light-soaked it under simulated AM 1.5 G intensity for 3.5 h. As shown in Figure 5B, the tape-treated half exhibited much better light stability, and the uniformity of the tape treatment is good, since no yellow spot was observed. We tested whether the speed of pressing and peeling was fast enough so that this can be integrated into a roll-to-roll fabrication line with a linear process speed in excess of 500 mm s^{-1}, the fast coating speed reported for scalable perovskite coating.[35] Therefore, the tape treatment holds great promise in scalable fabrication of stable and efficient perovskite solar modules.

Long-term operational stability of encapsulated RbCsFAMA perovskite devices were tested under a plasma lamp with a light intensity equivalent to AM 1.5 G in

Please cite this article in press as: Chen et al., Identifying the Soft Nature of Defective Perovskite Surface Layer and Its Removal Using a Facile Mechanical Approach, Joule (2020), https://doi.org/10.1016/j.joule.2020.10.014

air with a relative humidity of ~60 ± 10%.[36] The light source contained a substantial ultraviolet component and no ultraviolet filter was used during stability testing. All devices were loaded with a resistor so that they worked at maximum power point (MPP) at the beginning of the tests. Instead of monitoring device stability at a reduced temperature of ~25°C, which may cause an overestimation of solar cell stability,[37] we conducted the stability test at real operation temperature. Light illumination also heated the perovskite devices to ~65°C measured at the glass surface. The PCE of an encapsulated control device degraded rapidly from 19.1% to 14.7% after testing for 324 h (Figure 5C). On the contrary, the efficiency of a tape-treated device dropped only slightly to 97.1% of its initial efficiency after light soaking for 1,440 h. This is one of the most stable PSCs reported for those tested at real operation conditions.[12,36,38–42] Moreover, we measured the operational stability of another five tape-treated devices to check the reproductivity of our strategy. The stability data in Figure S17 show that all tape-treated devices retained 95.2% ± 1.9% of their initial efficiencies after light soaking for over 1,400 h. This indicates that the tape treatment method has a very good reproducibility and is, thus, promising for scalable manufacturing of perovskite modules.

Conclusion

In summary, we demonstrated a strategy to remove defective perovskite surfaces with low-cost adhesive tapes to stabilize perovskite films. This strategy also increased the PCEs of the perovskite devices up to 22.0%. The tape-treated device exhibited a long operational time of >1,400 h with negligible efficiency loss. Our studies have also shown the universality of this method in other commonly used perovskite compositions and the compatibility of this method with scaling up of perovskite photovoltaics. This method can also be broadly used in other thin-film perovskite electronic devices and eventually in all perovskite compositions.

EXPERIMENTAL PROCEDURES

Resource Availability

Lead Contact

Further information and requests for resources and materials should be directed to, and will be fulfilled by, the Lead Contact, Jinsong Huang (jhuang@unc.edu).

Materials Availability

This study did not generate new unique materials.

Data and Code Availability

This study did not generate any datasets or codes.

Materials

Poly(bis(4-phenyl)(2,4,6-trimethylphenyl)amine) (PTAA, average GPC M_n 7,000–10,000), bathocuproine (BCP), lead iodide (PbI_2, 99.999% trace metals), lead bromide ($PbBr_2$, 99.999% trace metals basis), tin (II) iodide (SnI_2, 99.99% trace metals basis), cesium iodide (CsI), rubidium iodide (RbI), *N*,*N*-dimethylformamide (DMF), 2-methoxyethanol (2-ME), dimethyl sulfoxide (DMSO), *L*-α-phosphatidylcholine (LP), 3-(decyldimethylammonio)-propane-sulfonate inner salt (DPSI), isopropanol (IPA), toluene, and chlorobenzene were purchased from Sigma-Aldrich and were used without further purification. Methylammonium iodide (MAI), methylammonium bromide (MABr) and formamidinium iodide (FAI) were purchased from GreatCell Solar. Methylammonium chloride (MACl) was purchased from Xi'an Polymer Light Technology Corp.

Please cite this article in press as: Chen et al., Identifying the Soft Nature of Defective Perovskite Surface Layer and Its Removal Using a Facile Mechanical Approach, Joule (2020), https://doi.org/10.1016/j.joule.2020.10.014

Device Fabrication

Patterned ITO glass substrates (1.5 × 1.5 cm) were first cleaned by ultrasonication with soap, deionized water and IPA, and then UV-ozone treated for 15 min before use. The hole transport layer PTAA with a concentration of 2 mg mL^{-1} (dissolved in toluene) was spin-coated onto ITO glass substrates at a speed of 5,000 rpm for 30 s and then annealed at 100°C for 10 min. The perovskite precursor solutions with different compositions were prepared and then deposited onto the PTAA-covered substrates according to the processing conditions detailed in Table S4. Except that the bladed films were prepared in ambient conditions (298 K and RH ~60%), the other films were all spin-coated in a N_2-filled glovebox. Surface treatment with adhesive tape was performed by pressing the tape (3M Temflex 1700 tape) onto the surface of perovskite films under a pressure of ~1 MPa and then slowly separating the tape from the film surface. This step can be repeated two or three times to further improve the uniformity of tape treatment. The devices were completed by thermally evaporating C_{60} (30 nm, 0.2 Å s^{-1}), BCP (6 nm, 0.1 Å s^{-1}), and copper (90 nm, 1 Å s^{-1}) in a sequential order. The device active area is 8 mm^2 determined by a shadow mask.

Device Characterization

The *J-V* characteristics of solar cells were performed using a Xenon-lamp-based solar simulator (Oriel Sol3A, Class AAA Solar Simulator) and the power of the simulated light was calibrated to 100 mW cm^{-2} using a silicon reference cell (Newport 91150V-KG5). All devices were measured using a Keithley 2400 source meter with a forward or backward scan rate of 0.1 V s^{-1} in air at room temperature, and the delay time was 10 ms. There was no preconditioning before measurement. A metal mask with an aperture (1.6 × 3.8 mm) aligned with the device area was used for measurements. The steady-state PCE was measured by monitoring current with the largest power output bias voltage and recording the value of the photocurrent. The tDOS of solar cells were derived from the frequency-dependent capacitance (C-f) and voltage-dependent capacitance (C-V), which were obtained from the thermal admittance spectroscopy (TAS) measurement performed by an LCR meter (Agilent E4980A). The transient photovoltage was measured under 1 sun illumination. An attenuated UV laser pulse (SRS NL 100 Nitrogen Laser) was used as a small perturbation to the background illumination on the device. The laser-pulse-induced photovoltage variation on V_{oc} is recorded by an Agilent Digital Storage Oscilloscope 3104A. The wavelength of the N_2 laser was 337 nm with a repeating frequency of about 10 Hz, and the pulse width was less than 4 ns.

Device Encapsulation

A thin layer of CYTOP was first blade-coated onto the back surface of the device, followed by thermal annealing at 70°C for 20 min on a hot plate. Then, a cover glass was attached onto the back surface for further protection by epoxy resin.

Device Operational Stability Test

Long-term stability measurements of encapsulated perovskite devices were operated under a plasma lamp with a light intensity equivalent to AM 1.5 G, without a UV filter, in air (relative humidity ~60% ± 10 %). The temperature of the devices under illumination was measured to be ~65°C. All devices were loaded with a resistor so that they worked at MPP at the beginning of the test. The *J-V* curves were recorded with a reverse scan rate of 0.1 V s^{-1}.

Structure Characterization

GIXRD measurements were carried out with a Rigaku SmartLab diffractometer using Cu Kα radiation (a wavelength of 1.5418 Å), and the height of films was calibrated

before each measurement. Cross-section FIB sample lamellae were prepared on a FEI Quanta 3D FEG DualBeam instrument. In this study, we started with a complete solar cell with both evaporated C60/BCP and Cu, and also a thick layer (>2 μm) of Pt was sputtered onto the device surface for the purpose of better protection. The sample was cut from the bulk material with a 30 kV ion beam and the last step was with a 3 nA current. During final thinning, the voltage was set to 16 kV and the currents used were 0.5 and 0.15 nA. Then, a final polish was done at 2 kV and 28 pA, which is lower than the threshold previously reported for the film samples without electrode protection.[43] Since our sample had been coated by heat-conductive materials of Cu and Pt, more heat will accumulate at the middle of the perovskite film than at the perovskite/electrode interface. As a result, the bulk of perovskite film would be damaged much more than the interfaces, if there was beam induced damage. The FIB lamellae were targeted with a final thickness of about 100 nm but this may vary locally. TEM was performed on a FEI Talos F200X analytical scanning transmission electron microscope operating at 200 kV and the bright-field TEM images were acquired in a low dose condition. The total electron dose was less than 100 e $Å^{-2}$. As suggested by previous work,[43] this is a safe dose for TEM imaging of $MAPbI_3$. During the bright-field TEM images acquisition period, we did not observe any phase change according to *in situ* fast Fourier transform (FFT). SEM images were taken on FEI Helios 600 Nanolab Dual Beam System operating at 5 or 20 kV, and EDS spectra were obtained with an EDS Oxford instrument (INCA PentaFET-x3). The AFM images were scanned from an Asylum Research MFP-3D Atomic Force Microscope under a tapping mode. The XPS was performed on a Kratos Axis Ultra DLD X-ray photoelectron spectrometer by using a monochromatized Al Kα source ($h\nu$ = 1,486.6 eV).

Mechanical Characterization

A Bruker Hysitron TI980 Triboindenter was utilized to perform both nanoscratch and nanoindentation on one-step spin-coated $MAPbI_3$ films using a three-sided diamond Berkovich tip. The Berkovich indenter tip was calibrated on quartz standards using a preliminary calibration procedure.

Ion-Migration Studies

Activation energy for ion migration was measured using a lateral device structure of glass/PTAA/perovskite/Au by a Keithley 2601 source meter at different temperatures. The electric field of the lateral device was 0.4 V $μm^{-1}$. The device was set in a Lakeshore Probe Station to obtain desired temperature.

PL Mapping

The PL mapping was conducted on a PicoQuant MT100 FLIM System at room temperature. A 485 nm laser (PicoQuant LDH-P-C-405B) pulsed at 1.5 MHz with an intensity of 0.89 sun per pulse was coupled into the confocal microscope and focused onto the sample. The PL mapping was conducted over a 10 × 10 μm region, and the PL intensity was recorded by a hybrid PMT detector.

SUPPLEMENTAL INFORMATION

Supplemental Information can be found online at https://doi.org/10.1016/j.joule.2020.10.014.

ACKNOWLEDGMENTS

This work is supported by the Center for Hybrid Organic Inorganic Semiconductors for Energy (CHOISE), an Energy Frontier Research Center funded by the Office of

Basic Energy Sciences, Office of Science within the U.S. Department of Energy and Office of Naval Research under award N00014-17-1-2727. tThe The TEM measurement was performed in part at the Analytical Instrumentation Facility (AIF) at North Carolina State University, which is supported by the State of North Carolina and the National Science Foundation (award number ECCS-1542015). We thank Dr. Shen Wang for XPS and part of SEM measurements.

AUTHOR CONTRIBUTIONS

S.C. and J.H. conceived the idea and designed the experiments. S.C. fabricated $MAPbI_3$, CsFAMA, and RbCsFAMA perovskite thin films and devices; measured their stabilities; and conducted and analyzed SEM/TEM results. Y.L. conducted nanoindentation and nanoscratch tests. X.X. measured GIXRD and TPV. Z.Y. fabricated wide- and narrow-band-gap perovskite devices. Y.D. assisted to blade $MAPbI_3$ perovskite films. X.D. conducted and analyzed AFM. Z.N. measured PL mapping and tDOS. S.C. and J.H. wrote the paper. All authors reviewed this paper.

DECLARATION OF INTERESTS

J.H., S.C., and Y.L. are inventors on a patent application related to this work filed by the University of North Carolina, Chapel Hill. The other authors declare no competing interests.

Received: September 15, 2020
Revised: October 9, 2020
Accepted: October 26, 2020
Published: December 16, 2020

REFERENCES

1. NREL (2020). Best Research-cell efficiency chart. https://www.nrel.gov/pv/cell-efficiency.html.
2. Christians, J.A., Habisreutinger, S.N., Berry, J.J., and Luther, J.M. (2018). Stability in perovskite photovoltaics: A paradigm for newfangled technologies. ACS Energy Lett. *3*, 2136–2143.
3. Kim, H.S., Hagfeldt, A., and Park, N.G. (2019). Morphological and compositional progress in halide perovskite solar cells. Chem. Commun. *55*, 1192–1200.
4. Chen, B., Rudd, P.N., Yang, S., Yuan, Y., and Huang, J. (2019). Imperfections and their passivation in halide perovskite solar cells. Chem. Soc. Rev. *48*, 3842–3867.
5. Wang, Y., Wu, T., Barbaud, J., Kong, W., Cui, D., Chen, H., Yang, X., and Han, L. (2019). Stabilizing heterostructures of soft perovskite semiconductors. Science *365*, 687–691.
6. Boyd, C.C., Cheacharoen, R., Leijtens, T., and McGehee, M.D. (2019). Understanding degradation mechanisms and improving stability of perovskite photovoltaics. Chem. Rev. *119*, 3418–3451.
7. Back, H., Kim, G., Kim, H., Nam, C.-Y., Kim, J., Kim, Y.R., Kim, T., Park, B., Durrant, J.R., and Lee, K. (2020). Highly stable inverted methylammonium lead tri-iodide perovskite solar cells achieved by surface re-crystallization. Energy Environ. Sci. *13*, 840–847.
8. Kong, W., Zhao, C., Xing, J., Zou, Y., Huang, T., Li, F., Yang, J., Yu, W., and Guo, C. (2020). Enhancing perovskite solar cell performance through femtosecond laser polishing. Sol. RRL *4*, 42–45.
9. Green, M.A., Ho-Baillie, A., and Snaith, H.J. (2014). The emergence of perovskite solar cells. Nat. Photonics *8*, 506–514.
10. Zhao, Y., and Zhu, K. (2016). Organic–inorganic hybrid lead halide perovskites for optoelectronic and electronic applications. Chem. Soc. Rev. *45*, 655–689.
11. Rong, Y., Hu, Y., Mei, A., Tan, H., Saidaminov, M.I., Seok, S.I., McGehee, M.D., Sargent, E.H., and Han, H. (2018). Challenges for commercializing perovskite solar cells. Science *361*, eaat8235.
12. Jung, E.H., Jeon, N.J., Park, E.Y., Moon, C.S., Shin, T.J., Yang, T.Y., Noh, J.H., and Seo, J. (2019). Efficient, stable and scalable perovskite solar cells using poly(3-hexylthiophene). Nature *567*, 511–515.
13. Min, H., Kim, M., Lee, S.U., Kim, H., Kim, G., Choi, K., Lee, J.H., and Seok, S.I. (2019). Efficient, stable solar cells by using inherent bandgap of α-phase formamidinium lead iodide. Science *366*, 749–753.
14. Chen, W., Wu, Y., Yue, Y., Liu, J., Zhang, W., Yang, X., Chen, H., Bi, E., Ashraful, I., Grätzel, M., et al. (2015). Efficient and stable large-area perovskite solar cells with inorganic charge extraction layers. Science *350*, 944–948.
15. Yuan, Y., and Huang, J. (2016). Ion migration in organometal trihalide perovskite and its impact on photovoltaic efficiency and stability. Acc. Chem. Res. *49*, 286–293.
16. Aristidou, N., Eames, C., Sanchez-Molina, I., Bu, X., Kosco, J., Islam, M.S., and Haque, S.A. (2017). Fast oxygen diffusion and iodide defects mediate oxygen-induced degradation of perovskite solar cells. Nat. Commun. *8*, 15218.
17. Tomastik, J., and Ctvrtlik, R. (2013). Nanoscratch test—a tool for evaluation of cohesive and adhesive properties of thin films and coatings. EPJ Web Conf. *48*, 00027.
18. Bai, Y., Lin, Y., Ren, L., Shi, X., Strounina, E., Deng, Y., Wang, Q., Fang, Y., Zheng, X., Lin, Y., et al. (2019). Oligomeric silica-wrapped perovskites enable synchronous defect passivation and grain stabilization for efficient and stable perovskite photovoltaics. ACS Energy Lett. *4*, 1231–1240.
19. Yu, J., Wang, M., and Lin, S. (2016). Probing the soft and nanoductile mechanical nature of single and polycrystalline organic–inorganic hybrid perovskites for flexible functional devices. ACS Nano *10*, 11044–11057.
20. Stavrakas, C., Zelewski, S.J., Frohna, K., Booker, E.P., Galkowski, K., Ji, K., Ruggeri, E., Mackowski, S., Kudrawiec, R., Plochocka, P., et al. (2019). Influence of grain size on phase transitions in halide perovskite films. Adv. Energy Mater. *9*.

21. 3M. 3M™ Temflex™ Vinyl Electrical Tape 1700. https://www.3m.com/3M/en_US/company-us/all-3m-products/~/3M-Temflex-Vinyl-Electrical-Tape-1700/?N=5002385+3294355723&rt=rud.

22. Ebnesajjad, S., and Landrock, A.H. (2015). Adhesives Technology Handbook, Third Edition (William Andrew Publishing), pp. 339–352.

23. Yuan, Y., Chae, J., Shao, Y., Wang, Q., Xiao, Z., Centrone, A., and Huang, J. (2015). Photovoltaic switching mechanism in lateral structure hybrid perovskite solar cells. Adv. Energy Mater. *5*, 572–574.

24. Xing, J., Wang, Q., Dong, Q., Yuan, Y., Fang, Y., and Huang, J. (2016). Ultrafast ion migration in hybrid perovskite polycrystalline thin films under light and suppression in single crystals. Phys. Chem. Chem. Phys. *18*, 30484–30490.

25. Mamun, A.A., Mohammed, Y., Ava, T.T., Namkoong, G., and Elmustafa, A.A. (2018). Influence of air degradation on morphology, crystal size and mechanical hardness of perovskite film. Mater. Lett. *229*, 167–170.

26. Wang, Q., Dong, Q., Li, T., Gruverman, A., and Huang, J. (2016). Thin insulating tunneling contacts for efficient and water-resistant perovskite solar cells. Adv. Mater. *28*, 6734–6739.

27. Zhao, Y., Wei, J., Li, H., Yan, Y., Zhou, W., Yu, D., and Zhao, Q. (2016). A polymer scaffold for self-healing perovskite solar cells. Nat. Commun. *7*, 10228.

28. Liu, F., Dong, Q., Wong, M.K., Djurišić, A.B., Ng, A., Ren, Z., Shen, Q., Surya, C., Chan, W.K., Wang, J., et al. (2016). Is excess PbI2 beneficial for perovskite solar cell performance? Adv. Energy Mater. *6*, 7849.

29. Roose, B., Dey, K., Chiang, Y.H., Friend, R.H., and Stranks, S.D. (2020). Critical assessment of the use of excess lead iodide in lead halide perovskite solar cells. J. Phys. Chem. Lett. *11*, 6505–6512.

30. Ciccioli, A., and Latini, A. (2018). Thermodynamics and the intrinsic stability of lead halide perovskites CH3NH3PbX3. J. Phys. Chem. Lett. *9*, 3756–3765.

31. Turren-Cruz, S.H., Hagfeldt, A., and Saliba, M. (2018). Methylammonium-free, high-performance, and stable perovskite solar cells on a planar architecture. Science *362*, 449–453.

32. Yang, Z., Yu, Z., Wei, H., Xiao, X., Ni, Z., Chen, B., Deng, Y., Habisreutinger, S.N., Chen, X., Wang, K., et al. (2019). Enhancing electron diffusion length in narrow-bandgap perovskites for efficient monolithic perovskite tandem solar cells. Nat. Commun. *10*, 4498.

33. Kapil, G., Bessho, T., Ng, C.H., Hamada, K., Pandey, M., Kamarudin, M.A., Hirotani, D., Kinoshita, T., Minemoto, T., Shen, Q., et al. (2019). Strain relaxation and light management in tin-lead perovskite solar cells to achieve high efficiencies. ACS Energy Lett. *4*, 1991–1998.

34. Lin, R., Xiao, K., Qin, Z., Han, Q., Zhang, C., Wei, M., Saidaminov, M.I., Gao, Y., Xu, J., Xiao, M., et al. (2019). Monolithic all-perovskite tandem solar cells with 24.8% efficiency exploiting comproportionation to suppress Sn(II) oxidation in precursor ink. Nat. Energy *4*, 864–873.

35. Deng, Y., Van Brackle, C.H., Dai, X., Zhao, J., Chen, B., and Huang, J. (2019). Tailoring solvent coordination for high-speed, room-temperature blading of perovskite photovoltaic films. Sci. Adv. *5*, eaax7537.

36. Yang, S., Chen, S., Mosconi, E., Fang, Y., Xiao, X., Wang, C., Zhou, Y., Yu, Z., Zhao, J., Gao, Y., et al. (2019). Stabilizing halide perovskite surfaces for solar cell operation with wide-bandgap lead oxysalts. Science *365*, 473–478.

37. Chen, B., Song, J., Dai, X., Liu, Y., Rudd, P.N., Hong, X., and Huang, J. (2019). Synergistic effect of elevated device temperature and excess charge carriers on the rapid light-induced degradation of perovskite solar cells. Adv. Mater. *31*, e1902413.

38. Christians, J.A., Schulz, P., Tinkham, J.S., Schloemer, T.H., Harvey, S.P., Tremolet de Villers, B.J., Sellinger, A., Berry, J.J., and Luther, J.M. (2018). Tailored interfaces of unencapsulated perovskite solar cells for >1,000 hour operational stability. Nat. Energy *3*, 68–74.

39. Arora, N., Dar, M.I., Hinderhofer, A., Pellet, N., Schreiber, F., Zakeeruddin, S.M., and Grätzel, M. (2017). Perovskite solar cells with CuSCN hole extraction layers yield stabilized efficiencies greater than 20%. Science *358*, 768–771.

40. Bai, S., Da, P., Li, C., Wang, Z., Yuan, Z., Fu, F., Kawecki, M., Liu, X., Sakai, N., Wang, J.T.-W., et al. (2019). Planar perovskite solar cells with long-term stability using ionic liquid additives. Nature *571*, 245–250.

41. Bi, D., Li, X., Milić, J.V., Kubicki, D.J., Pellet, N., Luo, J., LaGrange, T., Mettraux, P., Emsley, L., Zakeeruddin, S.M., et al. (2018). Multifunctional molecular modulators for perovskite solar cells with over 20% efficiency and high operational stability. Nat. Commun. *9*, 4482.

42. Wang, L., Zhou, H., Hu, J., Huang, B., Sun, M., Dong, B., Zheng, G., Huang, Y., Chen, Y., Li, L., et al. (2019). A Eu^{3+}-Eu^{2+} ion redox shuttle imparts operational durability to Pb-I perovskite solar cells. Science *363*, 265–270.

43. Rothmann, M.U., Li, W., Zhu, Y., Liu, A., Ku, Z., Bach, U., Etheridge, J., and Cheng, Y.B. (2018). Structural and chemical changes to CH3 NH3 PbI3 induced by electron and gallium ion beams. Adv. Mater. *30*, e1800629.